

# Evaluating the effect of building patterns on urban flooding based on a boosted regression tree: a case study of Beijing, China

Zhen Li<sup>1</sup>, Zhuowei Wang<sup>1</sup>, Leixiang Wu<sup>1</sup>, Wei Huang<sup>1</sup>, and Wenqi Peng<sup>1</sup>

<sup>1</sup>China Institute of Water Resources and Hydropower Research

January 20, 2023

## Abstract

Rapid urbanization and global climate change are likely to exacerbate urban flooding intensity, frequency, and uncertainty. Thus, it is fundamental and crucial to investigate the dominant influencing factors for the mitigation of urban flooding. However, the influence of building patterns on urban flooding remains limited. Taking Beijing, a typical megacity, as a case study area, we quantified the importance of building patterns and their interaction effect at the subwatershed scale using the boosted regression tree (BRT) and geographical detector model (GeoD). The results indicated that (1) the landscape shape index, slope, green space ratio and waterbody ratio were the most important influencing factors determining urban flooding, with a total relative contribution of 67.23%, (2) building metrics had a certain impact on urban flooding, and the sum of the relative contribution can reach 21.03%, (3) with urban flooding density, the landscape shape index, slope, and green space ratio exhibited a combination of negative and positive correlation, and (4) an enhancement effect existed between building metrics, especially the building congestion degree and building density. These findings provide quantitative insights that rational urban morphology planning can improve stormwater management and promote urban sustainability in megacities.



## 1. INTRODUCTION

Along with rapid urbanization, the proportion of world urban residents is expected to increase from 56.2% in 2020 to 67.2% in 2050 (DESA, 2018). It was estimated that global urban landscape area has increased by 19.1 million  $\text{hm}^2$  between 1985–2015, and approximately 70% of the newly urban landscape witnesses in Asia and North America (Liu et al., 2020). Unprecedented rate of global urbanization, whose most significant feature is the natural and semi natural surface being replaced by the impervious surface, causes a series of ecological challenges, such as urban flooding, urban heat islands, air pollution, and loss in natural habitat (Kulmala et al., 2020; Oke et al., 2017; Grimm et al., 2008; Foley et al., 2005). Urban flooding, refers to the fact that the heavy rainfalls overwhelm the capacity of self absorption and drainage pipelines drainage. Urban flooding causes great economic losses, and even kills the urban dwellers (Rentschler et al., 2022; Paprotny et al., 2018). It was reported that more than half of the world's population was affected by flooding from 2010

to 2019. China suffered from the flooding with 400 events contemporaneous. Meanwhile, global warming is likely to exacerbate urban flooding risks (Touma et al., 2022; Debele et al., 2019). Thus, how to reduce urban flood loss is of great significance to urban sustainability. Fortunately, a series of practices have been conducted, such as “best management practices”, “low impact development”, and “sponge city construction” (Davis et al., 2005).

Urban flooding has attracted more and more attention for its frequent occurrence and severe damage (Kim et al., 2022; Lin et al., 2022; Ma et al., 2022; Chen et al., 2021; Sun et al., 2021; Yang et al., 2021; Paprotny et al., 2018). Previous related studies have tended to reveal urban hydrological mechanism by adopting field investigations, laboratory modeling and urban hydrological modeling (Ma et al., 2022; Shrestha et al., 2022; Li et al., 2022; Muthusamy et al., 2021). Among these, a comprehensive understanding of the spatial-temporal patterns of urban flooding and its most influencing factors was vital and fundamental (Steinhausen et al., 2022; Li et al., 2022). Urban flooding events were significantly clustered and mainly distributed in the central urban area (Li et al., 2022; Zhang et al., 2020). The distribution pattern of urban flooding events can be caused by topographic conditions (i.e., elevation, slope, roughness, and microtopography), rainfall intensity, land cover composition and configuration, stormwater storages, and drainage systems (Hettiarachchi et al., 2022; Li et al., 2022; Wang et al., 2022; Dumedah et al., 2021; Liang et al., 2021). For example, Tehrani et al. (2019) found that elevation was significantly impacted urban flooding in small catchments. When the digital elevation model resolution increased from 50 m to 1 m, flooding extent and mean flood depth decreased by 30% and 150%, respectively (Muthusamy et al., 2021). However, it is difficult to alter topographic and heavy rainfall, so more and more researches seek to mitigate urban flooding through rational urban planning. On the one hand, an improvement in urban drainage system was beneficial to manage urban runoff. On the other hand, optimal blue-green-grey spaces were also important to alter urban hydrological process and reduce flooding risks.

Numerous studies have shown that land cover and land configuration have direct effects on urban flooding in the horizontal (Hettiarachchi et al., 2022; Wang et al., 2022; Li et al., 2020). However, fewer studies have investigated the impact of buildings on urban flooding in the vertical dimensions (i.e., building height and its heterogeneity). Although buildings and roads may have roughly the same permeable capacity, their roles in regulating urban runoff can vary greatly (Cao et al., 2021). Specifically, building height and building coverage ratio alter runoff generation time. Building facades increase the surface contact with raindrops and thus decrease runoff. In addition, the interaction effect of building and its surrounding miniature garden has direct effects on the ground runoff. Furthermore, buildings alter its surrounding microclimate, which has direct or indirect effect on soil moisture and evapotranspiration. Thus, three-dimensional building pattern might change the local hydrological process. Lin et al. (2021) noted that adding building metrics can better explain the probability of flooding occurrence in Shenzhen, especially the building coverage ratio.

A large number of three-dimensional building metrics have been developed to comprehensively characterize building patterns (Kedron et al., 2019; Liu et al., 2017). A series of studies further explored the relationship between three-dimensional building pattern and land surface temperature/air temperature, air pollution. However, the effect of 2D/3D building patterns on urban flooding remains unclear. We attempt to address the following two questions: (1) how urban flooding events affected by 2D/3D building patterns in megacities? And (2) does an enhancement effect exist between 3D building metrics? Addressing these questions can promote our further understanding on the role of buildings in urban flooding. Such understanding can provide insights for urban flooding mitigation.

## 2. DATA AND METHODS

### 2.1 Study area

Beijing (115°25'-117deg30' E, 39deg28'-41deg05' N), a typical megacity, is located in northern of North China Plain (Fig.1). It covers an area of 16.4 thousand km<sup>2</sup>. The climate of Beijing belongs to temperature continental monsoon climate. The annual precipitation is 600 mm, and 80% of precipitation is concentrated in summer. The western and northern of the study area lie on mountains, and the central city lies largely

on flat land. The main rivers are the Yongding River, Chaobai River, Jvma River, Beiyun River, and Jiyun River. Beijing has witnessed rapid urban sprawl in the horizontal and vertical dimensions since the reform and “opening up” policy. The urban built-up area increased 3130 km<sup>2</sup> from 1980 to 2018 (Yin et al., 2021). The oldest part of the city is mainly composed of ancient buildings with low building height within the second ring road, such as Sihe yuan. In 2020, more than 25 buildings were taller than 200 m. Beijing has undergone serious urban flooding. Although a large-scale drainage system was constructed, the city still faces the challenge of frequent urban flooding. For example, 79 people were killed and more than \$1.6 billion were lost in Beijing on July 21, 2012. With the renewal of drainage facilities and the development of sponge city construction, a heavy rainstorm caused 37 road collapses within the whole city on July 16, 2018. Based on previous studies (Liu et al., 2022), highly urbanized areas are the most vulnerable area to flooding. Therefore, it is still necessary to mitigation flooding risks through urban planning and management in highly urbanized areas.

## 2.2 Data sources

A total of 139 flood points from 2011 to 2021 were collected from the Water Resources Bureau of Beijing (Table 1). However, the available data only provide the address of the urban flooding events without accurate coordinates. Thus, we first vectorized these positions according to the occurrence types. When the urban flooding event occurred on the road, we determined the geometric center of the road as the position following the method recommended by Zhang et al. (2018) (Fig.2). Building footprint and floor number information in 2017 were collected from Baidu Maps (map.baidu.com) (Table 1). By referring to the Gaofen-1 image (chromatic sensor with 2 m resolution), the location of the buildings is highly accurate. The building floor height was set 3 m through the building design regulations. The overall accuracy of building height was beyond 85% according to field surveys, which is satisfying. The digital elevation model (DEM) with a resolution of 12.5 m was acquired from <https://search.asf.alaska.edu/>. The land use data in 2020 with a resolution of 10 m was produced by European Space Agency (ESA) (<https://viewer.esa-worldcover.org/worldcover>) (Fig.2). Then, the land use types were integrated into four categories: impervious surface, green space, waterbody, and farmland. The landscape indices were calculated by Fragstats 4.2 based on the land use data. In addition, other potential explanatory factors of rainfall and drainage capacities were utilized as independent variables to explain the urban flooding (Li et al., 2022). The average rainfall was calculated by the annual precipitation data obtained from the National Earth System Science Data Center (<http://www.geodata.cn/>). Due to lack of drainage system, distances to river and road density were used to represent urban drainage capacity (Li et al., 2022). The river data and road data were acquired from the National Geomatics Center of China (<http://www.ngcc.cn/>).

## 2.3 Subwatershed unit

Urban hydrology has complex natural-artificial features. Urban flooding was closely related to the watershed surface characteristics, such as topography, land cover and land configuration. Thus, it is suitable to explore the relationship between urban flooding and explanatory factors from the perspective of the subwatershed unit in considering urban hydrological processes. Previous studies have proposed the concept frame of “watershed-land” in the field of urban hydro-ecology, fully considering the hydrological watershed unit and easy connection with urban planning (Yu et al., 2018). Following the method recommended by Yu et al. (2018), the DEM data was utilized to divide the subwatershed units using the D8 algorithm. Finally, the study area was divided into 130 subwatershed units with an average area of 15.7 km<sup>2</sup> (Fig.1).

## 2.4 Subwatershed unit

Local Morman’s index in ArcGIS 10.3 was used to identify the distribution patterns of urban flooding points. The cluster types can be mainly divided into high-high agglomeration, low-low agglomeration, high-low agglomeration, and low-high agglomeration. The formula is as follows:

$$I = n \times \frac{(x_i - x) \times \sum W_{ij}(x_i - x)}{\sum (x_i - x)^2}$$

Where,  $I$  is the local Mornan’s index;  $x_i$  and  $\bar{x}$  are the observation and the average of all observations, respectively.

## 2.5 Landscape metrics

Numerous landscape metrics have been developed to measure landscape composition and configuration. Considering the ecological meaning and previous researches (Li et al., 2022a; Lin et al., 2021), five landscape metrics were selected, including: percentage of green space, percentage of water body, percentage of impervious surfaces, patch density, and landscape shape index (Table 2). For the three-dimensional building metrics, we adopted the building coverage ratio (BCR), building density (BD), building congestion degree (BCD), building height (BH), floor area ratio (FAR), 3D shape index (3DSI), and 3D fractals (3DF). The BCR, BH, and FAR were the most commonly adopted indicators in urban planning (Liu et al., 2021). 3DSI and 3DF were comprehensive indicators, which were based on the surface area and volume of buildings.

## 2.6 The boosted regression tree (BRT) analysis

The density of flooding hotspots was chosen as the response variable. First, we conducted Pearson correlation analysis to examine the relationship between the density of flooding hotspots and the explanatory factors. Before BRT analysis, Pearson correlation analysis was conducted between the explanatory factors. Pearson correlation analysis was effective to exclude multicollinearity between explanatory factors. Pearson correlation coefficient ranges from -1 to 1, indicating a positive/negative relationship and the strength.

The BRT has been widely applied in land science and urban heat island researches in recent years for its superior performance in explaining the complex relationship between response variable and explanatory factors (Sun et al., 2020; Elith et al., 2008). A BRT uses recursive binary splitting to generate a regression tree algorithm and then uses boosting to obtain the nonlinear relationship between the response and its predictor variables. When the correlation coefficient between two explanatory factors was  $>0.7$ , one of the predictor variable was removed. Finally, the percentage of impervious surface, population density, and floor area ratio were removed. Additionally, the BRT model also outputs partial dependency plots, which can concisely explain the marginal effects of the explanatory factors. The marginal effects represent the potential impact of the specific factor with other explanatory factors holds constant. With the BRTs, the contributions of the selected indicator were determined by the coefficients. The sum of the relative contribution was 100%. Development of the BRT models was based on `dismo` package of the R software. The main parameters of the BRT were set to 0.0001 (learning rate), 0.6 (bag fraction), 10 (tree complexity), and 10-fold cross validation.

## 2.7 Geographical detector model

The geographical detector model (GeoD) could identify the interactive effect between variables, which is a spatial analysis model based on the theory of spatial heterogeneity (Song et al., 2020). It assesses the strength of association between two variables by comparing the association which is defined as  $q$ , which ranging from 0 to 1. A large value in  $q$ , indicates the explanatory power is stronger. The formula is as follows:

$$q = 1 - \frac{1}{N\sigma^2} \sum_{h=1}^L N_h \sigma_h^2$$

Where,  $\sigma^2$  is the variance of the response variables;  $L$  is the number of category of the response variables;  $1, \dots, L$  is the study population of the response variables.

The  $q_{1 \cap 2}$ , which represents the interaction between the factors ( $q_1, q_2 \dots$ ), can be calculated by the interaction detector. The interaction effect can be divided into 5 categories, including: independent, nonlinear weaken (NW), nonlinear enhancement (NE), single-factor nonlinear weaken (SNW), double-factor enhancement (DE), and independent (I) (Yan et al., 2021). Additionally, the model requires category variables. Here, K-means method is used to convert the response and explanatory variables into category variables. Development of the GeoD models was based on the R-software, “GD 1.10” package.

### 3. RESULTS

#### 3.1 Distribution patterns of urban flooding points

From 2011 to 2021, urban flooding points were mainly of the districts Haidian and Fengtai (Fig.3). The low-density area of urban flooding points was mainly distributed in the edge of the study area. Interestingly, the historic districts of Beijing, such as Dongcheng and Xicheng districts, had fewer flooding points. Results of Local Morans I showed that the urban flooding hot spots were obvious (Fig.3). The hot spots were mainly distributed in Haidian and Fengtai districts, while cold spots were small and aggregated in northeast of the study area and dispersed in the southeastern part of the study area.

#### 3.2 Relative contributions of driving forces to urban flooding

Based on the two fitted BRT models (one for considering the driving forces without buildings, and another for considering all driving forces), the relative contributions of the explanatory factors to the urban flooding across the study area are presented in Fig. 4. The results indicate that landscape shape index, slope, green space ratio, and waterbody ratio play dominant roles in influencing the density of flooding hotspots, with total relative contributions reach at 82.36% in model without considering the buildings. Specifically, the relative contributions of landscape shape index, slope, green space ratio, and waterbody ratio are 38.19%, 25.5%, 11.13%, and 7.54%, respectively. The results are robust in model with considering all driving forces. However, we found that building metrics play a certain role, with total contributions is 21.03%. Among these building metrics, the relative contributions of the building congestion degree, building density, 3D shape index, and building coverage ratio exceed 3.76%. For the category levels, land cover configuration has the largest relative contribution (33.69%), whereas the drainage capacity has the least importance (3.87%). The importance of the topography, land cover composition, and 3D building morphology are nearly equal.

#### 3.3 Relative contributions of driving forces to urban flooding

The marginal effects of the six most important driving forces are shown in Fig. 5. With urban flooding density, the landscape shape index is complex, with a positive correlation ranging from 2.5 to 2.8 and a negative correlation ranging from 2.8 to 3.1. The slope shows a stepwise positive correlation with urban flooding density. As the green space ratio increased from 20% to 28%, the urban flooding density decreased from 0.010 to 0.005. The urban flooding density varies from 0 to 0.005 when the building congestion degree increases from 0.02 to 0.03. Building density experiences an initial increase and then stabilizes and finally drops.

#### 3.4 Interactive effect between 3D building metrics

Among the building metrics, the GeoD factor detector demonstrated that three-dimensional fractal was the most influential factors, followed by building density ( $q = 0.186$ ) and building congestion degree (0.176), then building height (0.153) (Table 3). The results were inconsistent with BRT analysis results, which also suggested occlusion effects in BRT model.

The GeoD interaction detector indicated that enhancement effect exist between building metrics. The interaction effect of building congestion degree with building density ( $BCD \cap BD$ ) was greater than that from the two sub-factors individually. Here, ' $\cap$ ' represents interactions. These finding indicated that the occurrence of urban flooding would be increased when the building congestion degree included building density. For building coverage ratio and building height, the interaction effect was double-factor enhancement, which suggested urban flooding risks would be enhanced when building coverage ratio included building height. The interaction effect was nonlinear between building height and three-dimensional fractal. It means that the explanatory power of the GD model would not increase when adding both into the model.

### 4. DISCUSSION

#### 4.1 Influencing factors

Urban hydrological processes have altered with urban development, and thus distribution pattern of flooding

points has changed (Chang et al., 2021; Zhao et al., 2014). In this study, we integrated a series of driving factors (i.e., topography, building metrics) and identified the major driving factors of urban flooding by adopting BRT method. The reasons for urban flooding are complex, including natural and anthropogenic factors. Through BRT analysis, land cover configuration has the greatest impact on flooding. The fragmentation of green spaces would increase occurrence of urban flooding events on a given land cover composition (Zhang et al., 2020). Higher fragmentation at landscape level might lead to serious urban flooding, and its role varied across different megacities in China (Li et al., 2022). In our study, it suggests that the optimal landscape shape index was nearly 2.8. The results were not consistent with previous studies, the difference was caused by the response variable selected, explanatory factors selected, analysis units, and analysis methods. Similarly, contribution of patch density was only 2.54%, which reflects the patch density was not important.

Through BRT analysis, land cover composition has important impact on flooding. Increasing the green space and waterbody could mitigate the flooding risks. It was also suggested that increase the impervious surfaces would be inevitably increase urban flooding risks. This is attributed to large difference between impervious surfaces and green-blue space (green space and waterbody). Specifically, it is difficult for waterflow to penetrate into the impervious surfaces. Additionally, less surface roughness of the impervious surface promotes rainwater flow and accumulation. On the contrary, urban green space can reduce runoff and regulate rainwater storage. This finding is consistent with case study in other cities (Zhang et al., 2020). Zhang et al. (2020) found that land composition plays a dominant role in determining urban floods with analysis scale range from 1 km to 5 km in metropolitan coastal cities of Guangzhou, China (Zhang et al., 2020).

Fewer studies explored the impact of the building metrics on urban flooding, and the importance of building has not yet been agreed. For example, Lin et al. (2022) found that 3D building metrics exert the greatest influence on urban flooding. Li et al. (2022) revealed 3D building metrics had slight impact on urban flooding. Our results suggested that 3D building morphology played an important role in urban flooding, and the contribution of 3D building morphology was equal to that of land cover composition. In fact, contributions of building congestion degree and building density reached at 6.35% and 4.81%, respectively. However, the current study also found that the importance of three-dimensional fractal and building height was relatively low? The possible reason was that green space is correlated with impervious surfaces, and impervious surfaces is highly correlated with building coverage ratio. Meanwhile, buildings with higher three-dimensional fractal generally occupy larger base area and taller building height. The green space, building height, and 3D fractal had occlusion effects on urban flooding and thereby the importance of building coverage ratio and building height became weaker.

## 4.2 Interaction effect between 3D landscape metrics

Although numerous studies conduct multivariate analysis in urban flooding by using traditional statistical methods (i.e., pearson correlation, logistic regression, partial least squares, structural equation model) or machine learning method (i.e., random forest), fewer studies explore the interaction effect among explanatory factors (Ma et al., 2022). Urban morphology was complex and high heterogeneous, especially in the vertical direction. Existing 3D landscape metrics was still insufficient to analysis the urban canopy. Thus, it was necessary to explore the interaction effect among 3D landscape metrics. For example, more and aggregation impervious surfaces tend to rise the land surface temperature in urban heat island field. However, high-rise building can mitigate heat island effect through improve surface roughness and cast more shadows (Sun et al., 2020). How to simultaneous adjust the impervious surfaces and building height became vital to alleviate heat island. In our study, we revealed that enhancement effect exist between 3D building metrics. In particularly, when the 3D fractal as an given value, it is important to reduce 3D shape index to avoid urban flooding risks.

## 4.3 Urban planning implications

Our results can provide guidance to optimize urban morphology for urban flooding risk management. This

study emphasize that land cover configuration was the dominant factor influencing the urban flooding. Therefore, it is necessary and important to properly allocate urban components (e.g., impervious surfaces, green space, and waterbody). As terms of the land use cover, with urban green space decreased and fragmented, rainwater runoff reduction rate decreased from 23% to 17% during the period 2000 to 2010 in Beijing (Zhang et al., 2015). Decreasing impervious surfaces and increasing urban green-blue spaces were beneficial for mitigating the urban flooding risks dramatically.

3D building patterns also have a certain impact on urban flooding. It is a good choice to control the floor area ratio under given 3D fractal. In generally, urban planners restrict building height strictly in Beijing. Buildings induced rainfall redistribution is expected to increase the peak flow and become more important with the increase of rainfall intensity (Cao et al., 2021). Thus, slowing down the building coverage ratio became another choice. In practice, green roofs were beneficial for urban stormwater regulation, and the runoff mitigation capacity varied with the spatial variability of green roofs and greening on effective roof surfaces in small urbanized catchments in Beijing (Yao et al., 2020). Additionally, 3D building landscape alters microclimate and changes rainfall pattern.

#### 4.4 Limitations and future research

There are some limitations in this study. When exploring the impact of urbanization on hydrological process, it is best to conduct research on the watershed level. This study only involved one single city (the developed urban areas), it needs to validate the results in other similar areas. Owing to coarse time resolution of urban flood records (2011–2021), we cannot accurately assess the relationship between the position of flooding events and rainfall intensity. Additionally, the amount and depth of flooding were unavailable, and thus hinder further comprehensively understanding the relationship between urban flood and its explanatory factors. Despite these limitations, this study provided quantitative insight into the nonlinear relationship and magnitude between the 3D building morphology and urban flooding.

### 5. CONCLUSIONS

This study identified the dominant influencing factors of urban flooding by integrating series driving forces (topography, drainage capacity, land cover composition, landscape configuration, building patterns) by adopting BRT model. Moreover, we further revealed the interaction effects among building metrics in Beijing’s central area by using GD method. The urban flooding points present a aggregation pattern, and was mainly concentrated in Haidian and Fengtai districts. The landscape shape index, slope, green space ratio, and waterbody ratio were the most important factors affecting urban flooding, with total relative contribution of 67.23. Building metrics has a certain impact on urban flooding, and sum of relative contribution can reach at 21.03%. Anymore, enhancement effect exist between building metrics, especially the building congestion degree and building density. The results also demonstrated the occlusion effects in BRT model. This study provides practical suggestions to improve stormwater management via optimizing urban morphology in 2D and 3D.

### ACKNOWLEDGEMENTS

This work was supported by the National Natural Science Foundation of China (No. 51879279).

### REFERENCES

- Cao, X., Qi, Y., Ni, G., 2021, Significant Impacts of Rainfall Redistribution through the Roof of Buildings on Urban Hydrology, *Journal of Hydrometeorology* **22** (4): 1007-1023. <https://dx.doi.org/10.1175/jhm-d-20-0220.1>
- Chang, C., Li, Y., Chen, Y., Huang, J. J., Zhang, Y., 2021, Advanced statistical analyses of urbanization impacts on heavy rainfall in the Beijing metropolitan area, *Urban Climate* **40** . <https://dx.doi.org/10.1016/j.uclim.2021.100987>
- Chen, X., Zhang, H., Chen, W., Huang, G., 2021, Urbanization and climate change impacts on future flood risk in the Pearl River Delta under shared socioeconomic pathways, *Science of the Total Environment* **762** .

<https://dx.doi.org/10.1016/j.scitotenv.2020.143144>

Davis, A. P., 2005, Green engineering principles promote low-impact development, *Environmental Science & Technology* **39** (16): 338A-344A. <https://dx.doi.org/10.1021/es053327e>

Debele, S. E., Kumar, P., Sahani, J., Marti-Cardona, B., Mickovski, S. B., Leo, L. S., Porcu, F., Bertini, F., Montesi, D., Vojinovic, Z., Di Sabatino, S., 2019, Nature-based solutions for hydro-meteorological hazards: Revised concepts, classification schemes and databases, *Environmental Research* **179** . <https://dx.doi.org/10.1016/j.envres.2019.108799>

DESA, U., 2018, World Urbanisation Prospects, 2018 Revision, *Retrieved from New York* .

Dumedah, G., Andam-Akorful, S. A., Ampofo, S. T., Abugri, I., 2021, Characterizing urban morphology types for surface runoff estimation in the Oforikrom Municipality of Ghana, *Journal of Hydrology-Regional Studies* **34** . <https://dx.doi.org/10.1016/j.ejrh.2021.100796>

Elith, J., Leathwick, J. R., Hastie, T., 2008, A working guide to boosted regression trees, *Journal of Animal Ecology* **77** (4): 802-813. <https://dx.doi.org/10.1111/j.1365-2656.2008.01390.x>

Foley, J. A., DeFries, R., Asner, G. P., Barford, C., Bonan, G., Carpenter, S. R., Chapin, F. S., Coe, M. T., Daily, G. C., Gibbs, H. K., Helkowski, J. H., Holloway, T., Howard, E. A., Kucharik, C. J., Monfreda, C., Patz, J. A., Prentice, I. C., Ramankutty, N., Snyder, P. K., 2005, Global consequences of land use, *Science* **309** (5734): 570-574. <https://dx.doi.org/10.1126/science.1111772>

Grimm, N. B., Faeth, S. H., Golubiewski, N. E., Redman, C. L., Wu, J., Bai, X., Briggs, J. M., 2008, Global change and the ecology of cities, *Science* **319** (5864): 756-760. <https://dx.doi.org/10.1126/science.1150195>

Hettiarachchi, S., Wasko, C., Sharma, A., 2022, Rethinking urban storm water management through resilience - The case for using green infrastructure in our warming world, *Cities* **128** . <https://dx.doi.org/10.1016/j.cities.2022.103789>

Kedron, P., Zhao, Y., Frazier, A. E., 2019, Three dimensional (3D) spatial metrics for objects, *Landscape Ecology* **34** (9): 2123-2132. <https://dx.doi.org/10.1007/s10980-019-00861-4>

Kim, J., Lee, J., Hwang, S., Kang, J., 2022, Urban flood adaptation and optimization for net-zero: Case study of Dongjak-gu, Seoul, *Journal of Hydrology-Regional Studies* **41** . <https://dx.doi.org/10.1016/j.ejrh.2022.101110>

Kulmala, M., Kokkonen, T. V., Pekkanen, J., Paatero, S., Petaja, T., Kerminen, V.-M., Ding, A., 2021, Opinion: Gigacity - a source of problems or the new way to sustainable development, *Atmospheric Chemistry and Physics* **21** (10): 8313-8322. <https://dx.doi.org/10.5194/acp-21-8313-2021>

Li, C., Liu, M., Hu, Y., Wang, H., Zhou, R., Wu, W., Wang, Y., 2022a, Spatial distribution patterns and potential exposure risks of urban floods in Chinese megacities, *Journal of Hydrology* **610** . <https://dx.doi.org/10.1016/j.jhydrol.2022.127838>

Li, L., Uyttenhove, P., Vaneetvelde, V., 2020, Planning green infrastructure to mitigate urban surface water flooding risk - A methodology to identify priority areas applied in the city of Ghent, *Landscape and Urban Planning* **194** . <https://dx.doi.org/10.1016/j.landurbplan.2019.103703>

Li, X., Erpicum, S., Mignot, E., Archambeau, P., Piroton, M., Dewals, B., 2022b, Laboratory modelling of urban flooding, *Scientific Data* **9** (1). <https://dx.doi.org/10.1038/s41597-022-01282-w>

Liang, R., Thyer, M. A., Maier, H. R., Dandy, G. C., Di Matteo, M., 2021, Optimising the design and real-time operation of systems of distributed stormwater storages to reduce urban flooding at the catchment scale, *Journal of Hydrology* **602** . <https://dx.doi.org/10.1016/j.jhydrol.2021.126787>

Lin, J., He, P., Yang, L., He, X., Lu, S., Liu, D., 2022, Predicting future urban waterlogging-prone areas by coupling the maximum entropy and FLUS model, *Sustainable Cities and Society* **80** .

<https://dx.doi.org/10.1016/j.scs.2022.103812>

Lin, J., He, X., Lu, S., Liu, D., He, P., 2021, Investigating the influence of three-dimensional building configuration on urban pluvial flooding using random forest algorithm, *Environmental Research* **196** . <https://dx.doi.org/10.1016/j.envres.2020.110438>

Liu, L., Sun, J., Lin, B., 2022, A large-scale waterlogging investigation in a megacity, *Natural Hazards* . <https://dx.doi.org/10.1007/s11069-022-05435-3>

Liu, M., Hu, Y.-M., Li, C.-L., 2017, Landscape metrics for three-dimensional urban building pattern recognition, *Applied Geography* **87**: 66-72. <https://dx.doi.org/10.1016/j.apgeog.2017.07.011>

Liu, X., Huang, Y., Xu, X., Li, X., Li, X., Ciais, P., Lin, P., Gong, K., Ziegler, A. D., Chen, A., Gong, P., Chen, J., Hu, G., Chen, Y., Wang, S., Wu, Q., Huang, K., Estes, L., Zeng, Z., 2020, High-spatiotemporal-resolution mapping of global urban change from 1985 to 2015, *Nature Sustainability* **3** (7): 564+. <https://dx.doi.org/10.1038/s41893-020-0521-x>

Ma, C., Qi, W., Xu, H., Zhao, K., 2022, An integrated quantitative framework to assess the impacts of disaster-inducing factors on causing urban flood, *Natural Hazards* . <https://dx.doi.org/10.1007/s11069-022-05375-y>

Muthusamy, M., Casado, M. R., Butler, D., Leinster, P., 2021, Understanding the effects of Digital Elevation Model resolution in urban fluvial flood modelling, *Journal of Hydrology* **596** . <https://dx.doi.org/10.1016/j.jhydrol.2021.126088>

Oke, T. R., Mills, G., Voogt, J., 2017, *Urban climates*, Cambridge University Press

Paprotny, D., Sebastian, A., Morales-Napoles, O., Jonkman, S. N., 2018, Trends in flood losses in Europe over the past 150 years, *Nature Communications* **9** . <https://dx.doi.org/10.1038/s41467-018-04253-1>

Rentschler, J., Salhab, M., Jafino, B. A., 2022, Flood exposure and poverty in 188 countries, *Nature Communications* **13** (1). <https://dx.doi.org/10.1038/s41467-022-30727-4>

Shrestha, A., Mascaro, G., Garcia, M., 2022, Effects of stormwater infrastructure data completeness and model resolution on urban flood modeling, *Journal of Hydrology* **607** . <https://dx.doi.org/10.1016/j.jhydrol.2022.127498>

Song, Y., Wang, J., Ge, Y., Xu, C., 2020, An optimal parameters-based geographical detector model enhances geographic characteristics of explanatory variables for spatial heterogeneity analysis: cases with different types of spatial data, *Giscience & Remote Sensing* **57** (5): 593-610. <https://dx.doi.org/10.1080/15481603.2020.1760434>

Steinhausen, M., Paprotny, D., Dottori, F., Sairam, N., Mentaschi, L., Alfieri, L., Luedtke, S., Kreibich, H., Schroeter, K., 2022, Drivers of future fluvial flood risk change for residential buildings in Europe, *Global Environmental Change-Human and Policy Dimensions* **76** . <https://dx.doi.org/10.1016/j.gloenvcha.2022.102559>

Sun, F., Liu, M., Wang, Y., Wang, H., Che, Y., 2020, The effects of 3D architectural patterns on the urban surface temperature at a neighborhood scale: Relative contributions and marginal effects, *Journal of Cleaner Production* **258** . <https://dx.doi.org/10.1016/j.jclepro.2020.120706>

Sun, X., Li, R., Shan, X., Xu, H., Wang, J., 2021, Assessment of climate change impacts and urban flood management schemes in central Shanghai, *International Journal of Disaster Risk Reduction* **65** . <https://dx.doi.org/10.1016/j.ijdrr.2021.102563>

Tehrany, M. S., Jones, S., Shabani, F., 2019, Identifying the essential flood conditioning factors for flood prone area mapping using machine learning techniques, *Catena* **175**: 174-192. <https://dx.doi.org/10.1016/j.catena.2018.12.011>

Touma, D., Stevenson, S., Swain, D. L., Singh, D., Kalashnikov, D. A., Huang, X., 2022, Climate change increases risk of extreme rainfall following wildfire in the western United States, *Science Advances* **8** (13). <https://dx.doi.org/10.1126/sciadv.abm0320>

Wang, Y., Zhang, X., Xu, J., Pan, G., Zhao, Y., Liu, Y., Liu, H., Liu, J., 2022, Accumulated impacts of imperviousness on surface and subsurface hydrology-continuous modelling at urban street block scale, *Journal of Hydrology* **608** . <https://dx.doi.org/10.1016/j.jhydrol.2022.127621>

Yan, H., Wang, K., Lin, T., Zhang, G. Q., Sun, C. G., Hu, X. Y., Ye, H., 2021, The Challenge of the Urban Compact Form: Three-Dimensional Index Construction and Urban Land Surface Temperature Impacts, *Remote Sensing* **13** (6): 23. <https://dx.doi.org/10.3390/rs13061067>

Yang, Q., Zheng, X., Jin, L., Lei, X., Shao, B., Chen, Y., 2021, Research Progress of Urban Floods under Climate Change and Urbanization: A Scientometric Analysis, *Buildings* **11** (12). <https://dx.doi.org/10.3390/buildings11120628>

Yin, C. L., Meng, F., Guo, L., Zhang, Y. X., Zhao, Z., Xing, H. Q., Yao, G. B., 2021, Extraction and Evolution Analysis of Urban Built-Up Areas in Beijing, 1984-2018, *Applied Spatial Analysis and Policy* . <https://dx.doi.org/10.1007/s12061-021-09374-7>

Zhang, B., Xie, G.-d., Li, N., Wang, S., 2015, Effect of urban green space changes on the role of rainwater runoff reduction in Beijing, China, *Landscape and Urban Planning* **140**: 8-16. <https://dx.doi.org/10.1016/j.landurbplan.2015.03.014>

Zhang, H., Cheng, J., Wu, Z., Li, C., Qin, J., Liu, T., 2018, Effects of Impervious Surface on the Spatial Distribution of Urban Waterlogging Risk Spots at Multiple Scales in Guangzhou, South China, *Sustainability* **10** (5). <https://dx.doi.org/10.3390/su10051589>

Zhang, Q., Wu, Z., Zhang, H., Dalla Fontana, G., Tarolli, P., 2020, Identifying dominant factors of waterlogging events in metropolitan coastal cities: The case study of Guangzhou, China, *Journal of Environmental Management* **271** . <https://dx.doi.org/10.1016/j.jenvman.2020.110951>

Zhao, J., Yu, K., Li, D., 2014, Spatial characteristics of local floods in Beijing urban area, *Urban Water Journal* **11** (7): 557-572. <https://dx.doi.org/10.1080/1573062x.2013.833636>

## TABLES

**Table 1** Details of the main data used in the study.

Data	Description	Source
Flooding points	flooding points from 2011 to 2021	the Water Resources Bureau of Beijing
Building data	Including building footprints and building height	Baidu Maps (map.baidu.com)
Land use data	10 m resolution, classified into 11 classes, such as: trees, cropland	European Space Agency (ESA) ( <a href="https://viewer.esaworldcover.org/worldcover">https://viewer.esaworldcover.org/worldcover</a> )

**Table 2** Summary of 2D/3D landscape metrics considered in this study.

Categories	Name	Description	Formulas
Topography	Average elevation	The average elevation in the subwatershed area.	$AE = average(elevation)$

Categories	Name	Description	Formulas
Drainage capacity	Distance to river	Average distance from each grid to the river in the subwatershed area.	$d = \sqrt{\sum_{i=1}^n (x_i - y_i)^2}$
Land cover composition	Road density	Ration of road area to the subwatershed area.	$Rd = \frac{A_{roads}}{S_{site}}$
	Green space ratio	The proportion of green space area to the total subwatershed area.	$GSR = \frac{A_{green\ space}}{S_{site}}$
	Waterbody ratio	The proportion of waterbody area to the total subwatershed area.	$WR = \frac{A_{waterbody}}{S_{site}}$
land cover configuration	Impervious surface ratio	The proportion of impervious area to the total subwatershed area.	$ISR = \frac{A_{impervious\ surfaces}}{S_{site}}$
	Patch density	The ratio of the number of patches to the total subwatershed area.	$PN = \frac{n_i}{A_{subwatershed}}$
3D building morphology	Landscape shape index	The shape index is a measure of the shape complexity.	$LSI = \frac{0.25E}{\sqrt{A_{subwatershed}}}$
	Building coverage ratio	Building coverage ratio of the subwatershed.	$BCR = \frac{\sum_{i=1}^n BSi}{S_{site}}$
	Building density	Number of buildings in the subwatershed.	$BD = \frac{N}{A}$
	Building congestion degree	The density of buildings in 3D space.	$BCD = \frac{\sum_{i=1}^n V_i}{\max(H_i) * A}$
	Building height	The area-weighted average building height.	$BH = \frac{\sum_{i=1}^n BSi * BH_i}{\sum_{i=1}^n BSi}$
	Floor area ratio 3D shape index 3D fractal	Building area unit area of the subwatershed. The degree of shape complexity. The compactness of the buildings.	$FAR = \frac{\sum_{i=1}^n c * F}{S_{site}}$ $3DSI = \frac{\sum_{i=1}^n (BSi + Li * BH_i)}{3 * v * \sqrt{3v/4\pi}}$ $\lg N(r) = -D \lg r + c$

Notes:  $x_i, y_i$  were coordinate;  $A_{roads}, A_{green\ space}, A_{impervious\ surfaces},$  and  $A_{waterbody}$  were the area of roads, green space, waterbody, and impervious surfaces;  $n_i$  was the number of patches;  $E$  was the length of the patches;  $BS_i$ : building projected area;  $n$ : the number of buildings;  $S_{site}$ : area of the subwatershed.  $BHi$ : height of building.  $F$ : floor of building.  $c$ : constant.  $Li$ : perimeter of the buildings.  $v$ : volume of buildings of the subwatershed.  $N(r)$ : number of none-empty boxes;  $r$ : scale;  $D$ : 3D fractal dimension.

**Table 3** Results of Geo-Dector interaction detector.

	BCR	BH	FAR	3DSI	3DF	BD	BCD
BCR	0.082						
BH	0.349DE	0.153					
FAR	0.197DE	0.329DE	0.100				
3DSI	0.221DE	0.315DE	0.362DE	0.074			
3DF	0.196NW	0.249NW	0.372DE	0.305NW	0.208		
BD	0.328DE	0.432DE	0.355DE	0.412DE	0.184NW	0.186	
BCD	0.313DE	0.309NW	0.381DE	0.294DE	0.121NW	0.415DE	0.176

**FIGURE LEGENDS**

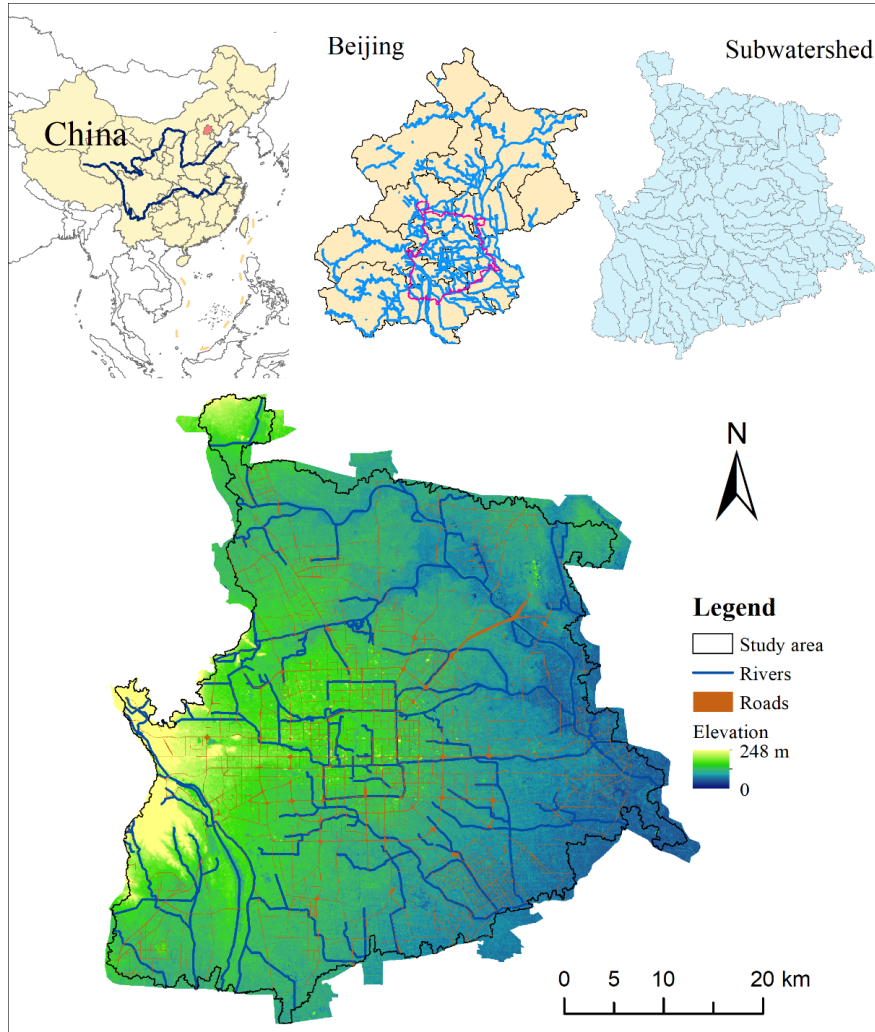


**Fig. 1** Geographic location, elevation, rivers, roads, and administrative boundaries of the study area.

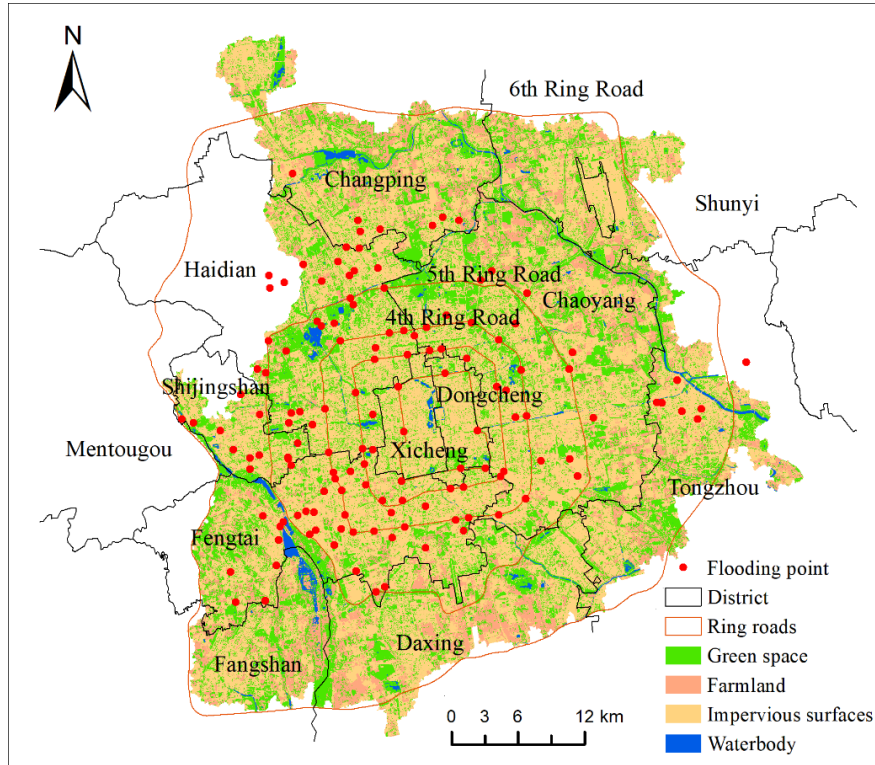


**Fig. 2** Spatial distributions of urban flooding points from 2011 to 2021.

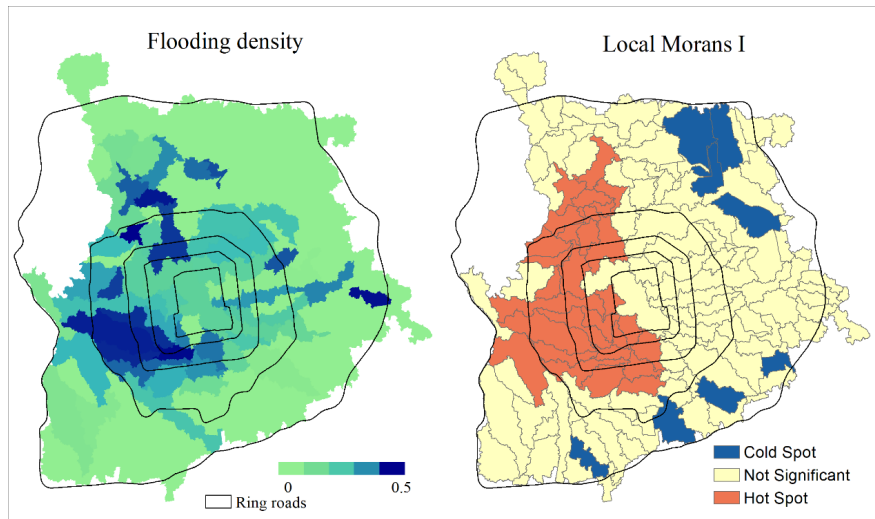


**Fig. 3** Spatial distribution of urban flooding density.

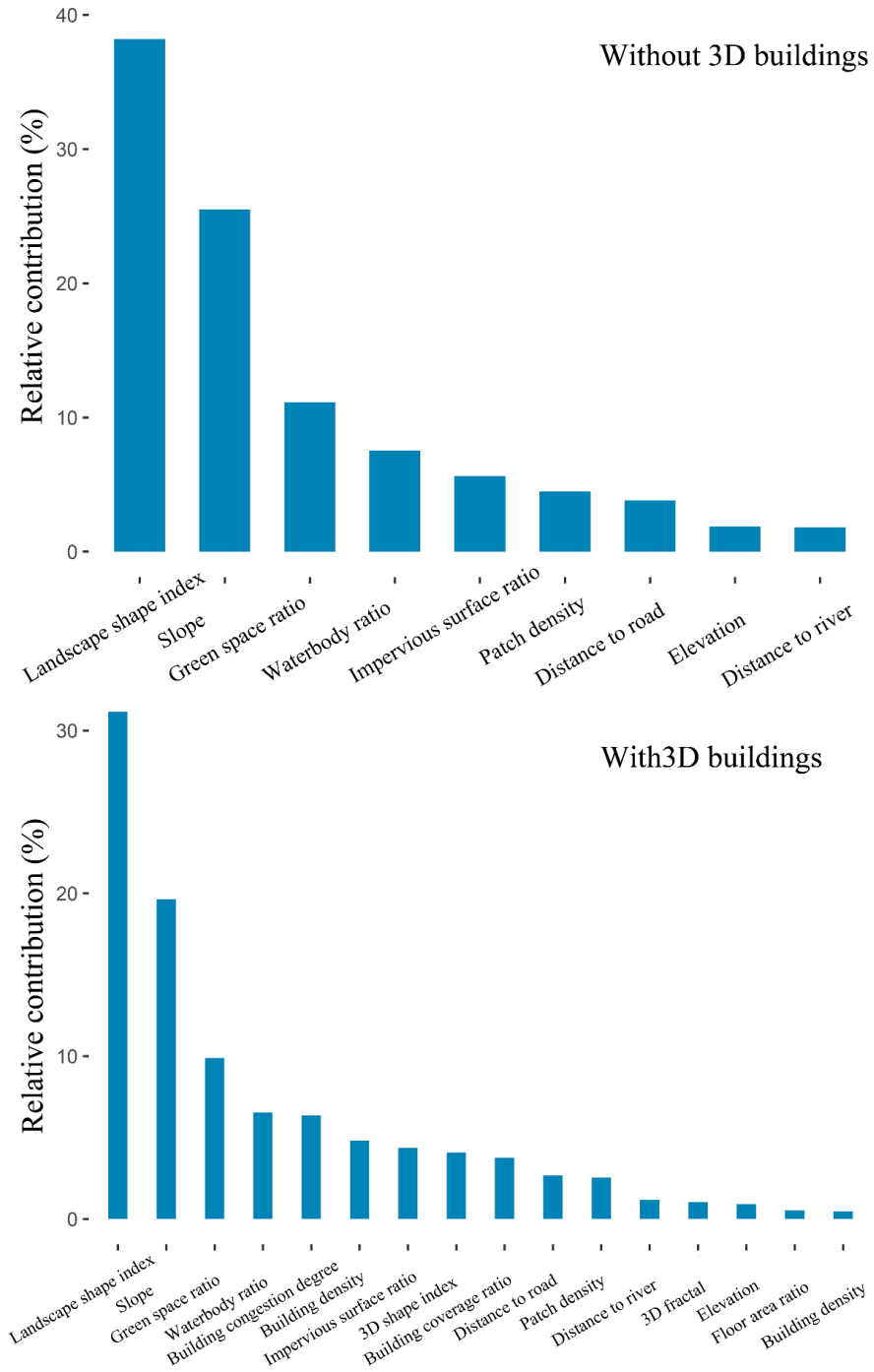


**Fig. 4** Relative contributions (%) of the influencing factors (without and with considering buildings) on urban flooding in Beijing.

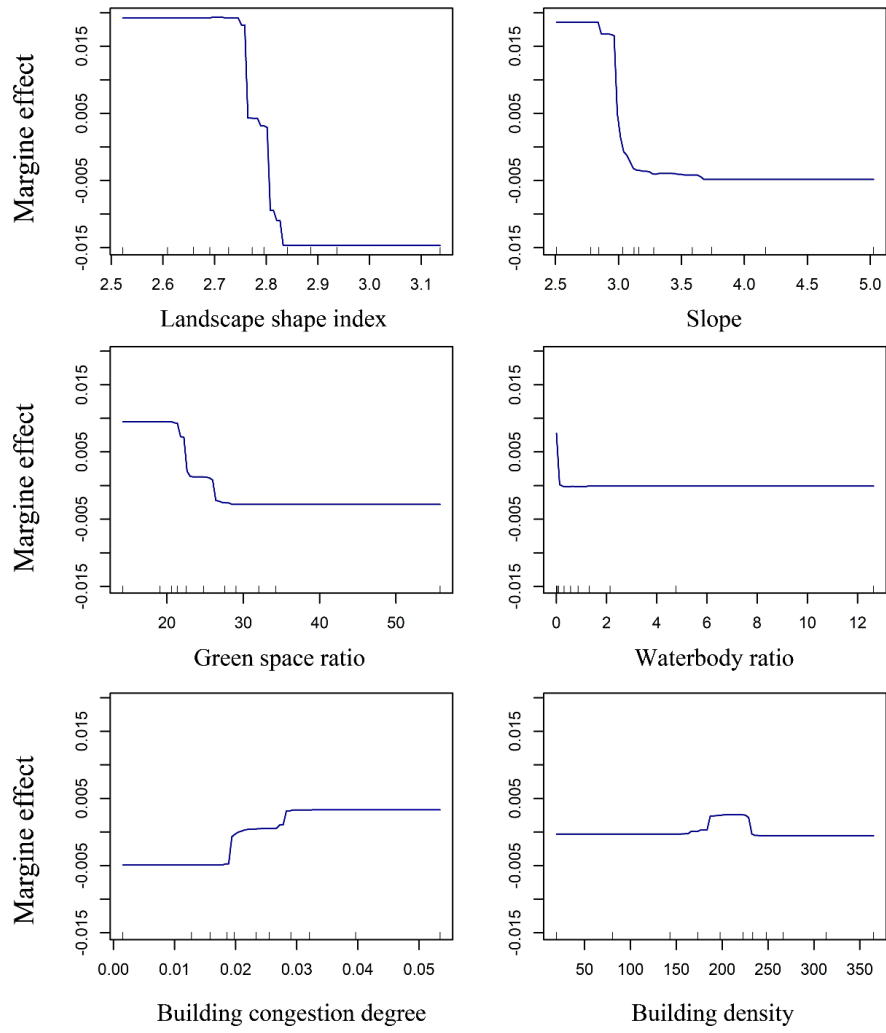


**Fig. 5** Marginal effects of the six most important explanatory variables in model considering all driving forces.